Shape transitions and collective excitations in ^{152}Dy

J. Kvasil,[1] N. Lo Iudice,[2] F. Andreozzi,[2] F. Knapp,[1] and A. Porrino[2]
[1]*Institute of Particle and Nuclear Physics, Charles University, V. Holesovickách 2, CZ-18000 Praha 8, Czech Republic*
[2]*Dipartimento di Scienze Fisiche, Universitá di Napoli, "Federico II" and Istituto Nazionale di Fisica Nucleare, Monte S. Angelo, Via Cinthia I-80126 Napoli, Italy*
(Received 24 November 2005; published 9 March 2006)

We adopt a self-consistent cranked Nilsson plus quasiparticle random-phase approximation by using a Hamiltonian of separable form to study the collective properties of ^{152}Dy as it evolves toward the superdeformed shape. Our calculation, while confirming the octupole character of the negative-parity superdeformed bands, emphasizes the effect of the new shell structure, induced by fast rotation combined with large deformation, on the other collective modes. It shows, in particular, that superdeformation enhances strongly the collectivity of the low-lying scissors mode built on the superdeformed shape.

DOI: 10.1103/PhysRevC.73.034302   PACS number(s): 21.60.Jz, 05.70.Fh, 27.70.+q, 21.10.Re

I. INTRODUCTION

The discovery of superdeformed (SD) rotational bands [1] has opened new perspectives in the study of nuclei under extreme conditions of fast rotation and large deformation. Under their combined action, novel shell structures emerge. In fact, new shell gaps in the single-particle spectra originate from the onset of degeneracy of normal-parity orbitals and from the redistribution and filling of several high-j intruders near the Fermi level [2,3].

Because of the modified shell structure, collective modes in SD nuclei are expected to exhibit new features with respect to the normal deformed phase. The literature on this subject, however, is not very rich. One of the few theoretical investigations is a microscopic analysis of collective SD bands in ^{152}Dy [4] and ^{190,192,194}Hg [5]. These authors, developing earlier preliminary studies [6], performed a microscopic calculation in a cranked Nilsson plus quasiparticle random-phase approximation (QRPA) by using separable dipole-dipole plus octupole-octupole interactions for the negative-parity SD bands and a quadrupole-quadrupole potential for the positive-parity states. The comparative analysis of computed and empirical dynamical moments of inertia led to the conclusion that octupole correlations characterize most of the low-lying excited SD bands.

An earlier study was focused on the properties of the magnetic dipole excitations [7]. The authors of Ref. [7] computed the magnetic dipole spectrum in the SD ^{152}Dy and ^{192}Hg in the QRPA by using a Woods-Saxon mean field plus quadrupole-quadrupole and spin-spin separable interactions. They showed that the spin response is dominant in the low-energy region at normal deformation. In going to the SD phase, however, the orbital response is strongly enhanced and becomes dominant even at low energy. These low-lying $M1$ excitations should then be associated with the low-lying scissors mode [8,9], extensively studied experimentally and theoretically for normally deformed nuclei [10].

At high energy, the $M1$ transitions are localized in the region of the isovector quadrupole giant resonance. They are purely orbital and therefore correspond to the high-energy scissors mode [11]. These $M1$ transitions become overwhelmingly strong in the SD phase and, because of their orbital nature, are to be considered as the *true* representatives of the scissors mode in SD nuclei. This association is further strengthened by the large overlap of the high-energy RPA eigenvectors with the schematic orbital scissors state.

As admitted explicitly by the authors [7], however, the effect of fast rotation on the mode is neglected. On the other hand, a recent calculation on nuclei undergoing backbending has proved the dramatic effect of rotation on magnetic dipole scissorslike excitations [12]. Moreover, the single-particle space adopted is too restricted to properly account for the spreading of the high energy strength.

In this paper, we study the combined action of fast rotation and large deformation on both positive- and negative-parity collective modes. More specifically, we analyze the octupole correlations and their effect on the dynamical moment of inertia. We also investigate how the properties of the other $E\lambda$ ($\lambda = 0, 1, 2$) collective modes change with increasing deformation and angular frequency. These transitions were studied previously in a schematic model [13]. We then focus our attention on the magnetic dipole $M1$ response and show how the collectivity of the low-lying $M1$ levels changes its nature and is dramatically enhanced with the onset of superdeformation.

Our procedure parallels the one we followed in Ref. [12]. We adopt a cranked Nilsson plus QRPA by using an interaction of general separable form, as in [4,5]. Such an approach is shown to lead to a restoration of the symmetries violated by external, mean, and BCS pairing fields, thereby ensuring the separation of the spurious or redundant modes from the physical excitations. The cranked shell model plus RPA was developed long ago [14] and applied extensively to high-spin collective modes [15–24].

II. BRIEF OUTLINE OF THE METHOD

As in Ref. [12], we adopt the Hamiltonian

$$H_\Omega = H_0(\Omega) + V_{PP} + V_{FF}, \tag{1}$$

where $H_0(\Omega)$ is a cranked Nilsson Hamiltonian, V_{PP} is a proton-proton and neutron-neutron monopole pairing, and V_{FF} is a sum of isoscalar and isovector separable potentials.

The cranked term has the structure

$$H_0(\Omega) = H_0 - \sum_{\tau=n,p} \lambda_\tau N_\tau - \hbar\Omega I_1, \qquad (2)$$

where the unperturbed term H_0 consists of two pieces. The first is a modified triaxial harmonic-oscillator (HO) Nilsson Hamiltonian, whose HO frequencies satisfy the volume-conserving condition

$$\omega_1\omega_2\omega_3 = \omega_0^3. \qquad (3)$$

The second term restores the local Galilean invariance broken in the rotating coordinate system and has the form given in Refs. [5,12,25].

At $\Omega = 0$, one may determine the equilibrium deformation by minimizing the expectation value of the one-body Hamiltonian H_0 with respect to the frequencies ω_i under volume-conserving constraint (3). This prescription is equivalent to a Hartree mean-field approximation applied to a system of nucleons interacting by means of many-body forces [26,27].

The two-body separable potential has the following structure:

$$V = \sum_{\lambda\mu} \kappa_\lambda F''^2_{\lambda\mu}, \qquad (4)$$

where the sum includes quadrupole-quadrupole plus monopole-monopole plus spin-spin separable potentials for positive-parity states and dipole-dipole plus octupole-octupole interactions for the negative-parity bands.

All multipole and spin-multipole fields $F''_{\lambda\mu}$ have good isospin T and signature r [28]. They are expressed in terms of doubly stretched coordinates $x''_i = (\omega_i/\omega_0)\, x_i$ [29,30] that, for a pure HO one-body Hamiltonian, ensure the self-consistent conditions

$$\langle Q''_\mu \rangle = 0, \quad \mu = 0, 1, 2, \qquad (5)$$

for the quadrupole field, at the equilibrium deformation. By virtue of Eqs. (5), the deformed mean field is not distorted further by the interaction and makes possible the separation of the spurious from the physical RPA solutions. Once expressed in these new coordinates, the λ fields no longer have a well-defined tensor rank and therefore alter the structure of the original separable interaction. Thus the unfolding of the doubly stretched fields yield dipole-octupole or monopole-quadrupole mixed interactions.

We make use of the generalized Bogoliubov transformation to express Hamiltonian (1) in terms of quasiparticle creation and annihilation operators. We then plug the transformed Hamiltonian into the RPA equations of motion, written in the form [28]

$$\begin{aligned} &[H_\Omega, P_\nu] = i\hbar\omega_\nu^2 X_\nu, \quad [H_\Omega, X_\nu] = -i\hbar\, P_\nu, \\ &[X_\nu, P_{\nu'}] = i\hbar\delta_{\nu\nu'}, \end{aligned} \qquad (6)$$

where X_ν and P_ν are, respectively, the collective coordinates and their conjugate momenta.

Exploiting the symmetries of the cranked Hamiltonian, we solve RPA eigenvalue equations (6) separately for the positive and negative signature pieces, $H_\Omega(+)$ and $H_\Omega(-)$, respectively, under the constraints [12]

$$\begin{aligned} &\left[H_\Omega\left(\substack{\pi=+\\ r=+}\right),\, N_\tau\right] = 0, \quad \left[H_\Omega\left(\substack{\pi=-\\ r=+}\right),\, P_1\right] = 0, \\ &\left[H_\Omega\left(\substack{\pi=+\\ r=+}\right),\, I_1\right] = 0, \quad \left[H_\Omega\left(\substack{\pi=+\\ r=-}\right),\, \Gamma^\dagger\right] = \Omega\Gamma^\dagger, \end{aligned} \qquad (7)$$

where $\tau = p, n$, and

$$\begin{aligned} \Gamma^\dagger &= \frac{1}{\sqrt{2\langle I_1 \rangle}}(I_2 + iI_3), \\ \Gamma &= (\Gamma^\dagger)^\dagger = \frac{1}{\sqrt{2\langle I_1 \rangle}}(I_2 - iI_3) \end{aligned} \qquad (8)$$

satisfy the commutation relation

$$[\Gamma, \Gamma^\dagger] = 1. \qquad (9)$$

According to Eqs. (7), we have three Goldstone modes. One is associated with the violation of the particle-number operator; the other two are zero-frequency translational and rotational solutions related to the breaking of translational and spherical symmetries of the mean field, respectively. The last equation yields a negative signature solution of energy $\omega_\lambda = \Omega$, which describes a collective rotational mode arising from the symmetries broken by the external rotational field (the cranking term).

Equations (7), if fulfilled, ensure the separation of the spurious or redundant solutions from the intrinsic ones. They would be automatically satisfied if the single-particle basis were generated by means of a self-consistent Hartree-Bogoliubov (HB) calculation. As we shall see, they are fulfilled with good accuracy also in our, not explicitly self-consistent, minimization procedure under volume-conserving constraint (3). Such a constraint was shown to be essential for obtaining the correct equilibrium deformations [26,27].

The strength function for an electric ($X = E$) or magnetic ($X = M$) transition of multipolarity λ from a state of the yrast line with angular momentum I is

$$S_{X\lambda}(E) = \sum_{\nu I'} B(X\lambda,\ I \rightarrow\ I',\ \nu)\, \delta(E - \hbar\omega_\nu), \qquad (10)$$

where $B(X\lambda,\ I \rightarrow\ I',\ \nu)$ is the reduced strength. The strength function method avoids the explicit determination of the RPA eigenvalues and eigenfunctions [28]. We just have to replace the δ distribution with a Lorentzian weight. Thus, on use of the Cauchy theorem, we obtain for $S_{X\lambda}(E)$ expressions involving only two quasiparticle matrix elements of one-body multipole operators.

The nth moments are obtained simply as

$$m_n(X\lambda) = \int_0^\infty E^n S_{X\lambda}(E)\, dE. \qquad (11)$$

The $m_0(X\lambda)$ and $m_1(X\lambda)$ moments give, respectively, the energy-unweighted and energy-weighted summed strengths.

To compute the strength function, we should be able to expand the intrinsic RPA states into components with good K quantum numbers, which is practically impossible in the cranking approach. We therefore compute the strength in the limits of zero and high angular frequencies (see Ref. [12] for details), taking into account the energy shift

$$\sum_{\mu} S_{X\lambda\mu}(E) \rightarrow \sum_{\mu} S_{X\lambda\mu}(E - \mu\hbar\Omega) \qquad (12)$$

in each μth component of the $X\lambda$ transition operator, where $\mu = \Delta I = I - I_{\rm yrast}$, in going from the intrinsic to the laboratory frame [17,18].

III. NUMERICAL PROCEDURE

In Ref. [12], we took the parameters of the Nilsson potential from Ref. [31], where they were determined from a systematic analysis of the experimental single-particle levels of deformed nuclei of rare earth and actinide regions at low rotational frequency.

To properly describe the single-particle properties at high spins and superdeformation, it would be necessary to adopt the Strutinsky shell correction method, since in SD nuclei the liquid-drop energy is large and necessary for determining the equilibrium deformation. This was the procedure adopted in Refs. [2] and [3] for a Woods-Saxon and a Nilsson Hamiltonian, respectively. In our simplified approach, we change the Nisson parameters of Ref. [31] so as to obtain at each Ω a set of single-particle energies close to the ones determined in a Nilsson-Strutinsky approach [32] and adopted in Ref. [3]. We thus obtain the new parameters $\kappa = 0.0637$, $\mu = 0.75$ and $\kappa = 0.064$, $\mu = 0.9$ for the major neutron shells $N = 6$ and $N = 7$, respectively, instead of $\kappa = 0.0637$, $\mu = 0.393$, adopted in [31] for both $N = 6$ and $N = 7$ neutron shells. We also use the new values $\kappa = 0.0620$, $\mu = 0.9$, instead of $\kappa = 0.0620$, $\mu = 0.614$ [31], for the $N = 7$ proton shell. We include all shells up to $N = 8$. Using these new parameters, we reproduce also the energy gaps for $Z = 66$ and $N = 86$ and the particle-like $N = 7$ single-particle intruder states just above the Fermi level obtained in [4,5].

The quite pronounced changes of the l^2 parameters μ are to be noted. These changes represent, partly, the price we have to pay to reproduce the single-particle energies of the Nilsson-Strutinsky approach and, partly, these changes are justified by the different treatment of the Nilsson potential. We use, in fact, the *unstretched* Nilsson scheme and account fully for the interactions between all $\Delta N \neq 0$ shells, while, in Refs. [4,5,32], *singly stretched* coordinates are adopted and the $\Delta N \neq 0$ coupling is neglected.

As in [12], we determine the pairing gaps following the phenomenological prescription [33]:

$$\Delta_\tau(\Omega) = \begin{cases} \Delta_\tau(0)\left[1 - \frac{1}{2}\left(\frac{\Omega}{\Omega_c}\right)^2\right], & \Omega < \Omega_c \\ \Delta_\tau(0)\frac{1}{2}\left(\frac{\Omega_c}{\Omega}\right)^2, & \Omega > \Omega_c \end{cases}, \qquad (13)$$

where Ω_c is the critical rotational frequency of the first band crossing. This empirical procedure avoids unwanted singularities one would encounter in correspondence to the critical frequencies within a pure self-consistent approach. We deduce the pairing gaps at zero rotational frequency from the odd-even mass differences, obtaining $\Delta_n(0) = 0.771$ MeV and $\Delta_p(0) = 1.09$ MeV.

IV. EQUILIBRIUM DEFORMATIONS AND SHAPE TRANSITIONS

We use the BCS vacuum to compute the expectation value of cranked Nilsson Hamiltonian (2) plus the pairing potential for several values of Ω under the volume-conserving constraint.

The β-γ contour plot in Fig. 1 shows that, for each Ω, we have two minima, one corresponding to $\beta \approx 0.2$, $\gamma = 0$ (normal deformation) and the other to $\beta \approx 0.5$–0.6, $\gamma = 0$ (superdeformation). A more detailed analysis shows that the absolute minimum is the one at normal deformation up to the rotational frequency $\hbar\Omega \approx 0.67$, while the SD minimum becomes deepest for $\hbar\Omega > 0.67$ and moves smoothly from $\beta = 0.53$ at $\hbar\Omega = 0.67$ to $\beta = 0.6$ at $\hbar\Omega = 0.8$. In other words, $\hbar\Omega \approx 0.67$ is a critical rotational frequency that marks the transition from deformed to SD shapes along the yrast line. This conclusion agrees with the results obtained in the Strutinsky shell correction calculations [2,3]. The similarity of the two results is due to the new Nilsson parameters, chosen so as to reproduce the single-particle energies used in Ref. [3], which amplify the effect of the l^2 term in shaping the single-particle spectrum. Such a change may represent a critical point. It was shown, in fact, that the energy minimum is sensitive to the details of the Nilsson Hamiltonian and, in particular, to the l^2 term and the way it is treated [34]. On the other hand, we have checked that the collective responses are not highly sensitive to these changes.

Alternatively, the equilibrium deformations may be determined by self-consistent conditions (5),

$$\langle Q''_{2\mu}\rangle_\Omega = \langle\Omega|\, Q''_{2\mu}|\Omega\rangle = 0, \quad \mu = 0, 2, \qquad (14)$$

at each Ω. As pointed out already, these zeros correspond to the energy minima of the HO Hamiltonian under the volume-conserving constraint [26,27]. The plots in Fig. 2 show that, for $\gamma = 0$, $\langle Q''_{20}\rangle_\Omega$ has two zeros for all rotational frequencies up

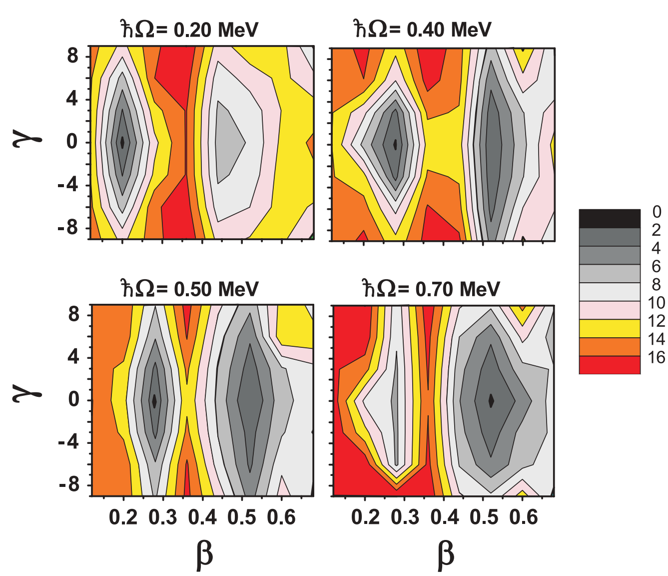

FIG. 1. (Color online) The β and γ contour plots of the cranked Nilsson plus pairing energy surfaces at different rotational frequencies Ω in ^{152}Dy. The surfaces give the relative energies $E(\beta,\gamma) - E_{\rm min}$.

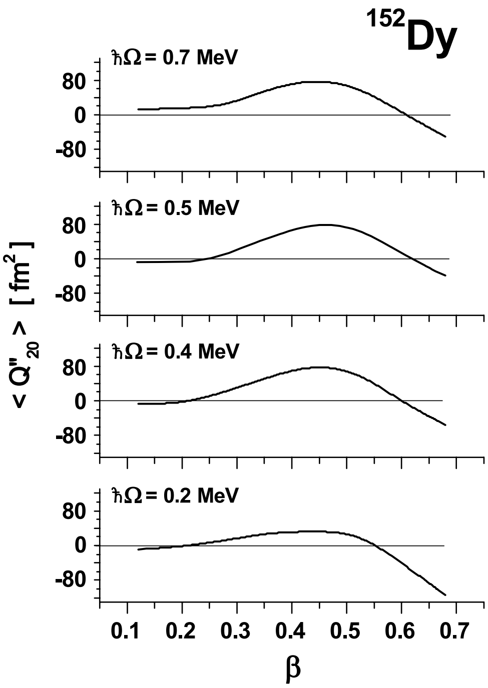

FIG. 2. The expectation value of the doubly stretched quadrupole moment versus β at different Ω's.

to $\hbar\Omega = 0.7$ MeV. In correspondence to this latter frequency, the doubly stretched quadrupole moment vanishes at only the SD value $\beta \approx 0.6$ and is very small (but not vanishing) in correspondence to the low deformation minimum, which becomes unstable toward triaxial deformation (Fig. 1).

From inspecting the two figures, one can see that the zeros of $\langle Q''_{2\mu}\rangle_\Omega$ do not coincide with the minima of the energy surfaces, as they should for a pure HO Hamiltonian, under the volume-conserving constraint. Apparently the minima are sensitive to the extra terms of the Nilsson Hamiltonian and, in particular, to the $\langle l^2\rangle$ piece [34], which in our case is amplified by the large parameters of μ adopted. Although not coinciding, the zeros are close to the energy minina for several values of Ω, suggesting that our equilibrium deformations are not far from the self-consistent ones.

The validity of our treatment is provided by its success in describing the angular-momentum expectation value, $\langle I_x\rangle_\Omega = \langle\Omega|I_x|\Omega\rangle$, along the yrast line. As shown in Fig. 3, the calculation reproduces fairly well the experimental angular momenta extracted from the energy levels of the yrast line through the formula

$$\hbar\Omega(I) = \frac{E_{\mathrm{yr}}(I+2) - E_{\mathrm{yr}}(I)}{2}, \tag{15}$$

where the energies are taken from experiments [35].

We observe a first shape transition, $\beta = 0.2 \to \beta = 0.28$, for $\hbar\Omega \approx 0.3$ MeV corresponding to the first backbending, then a second one, $\beta \approx 0.28 \to \beta \approx 0.6$, connected with the second backbending at $\hbar\Omega \approx 0.67$ MeV. For $\hbar\Omega > 0.66$ MeV, the SD yrast band, which we denote by SD1 according to the labeling adopted in Ref. [4], becomes the yrast line.

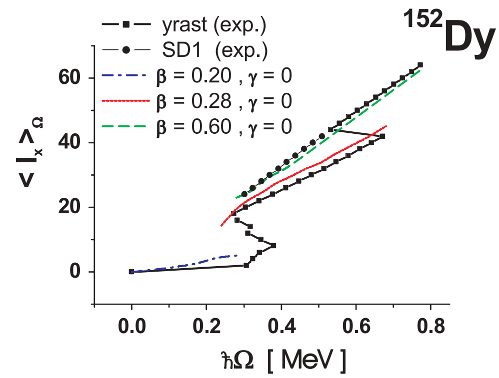

FIG. 3. (Color online) Yrast line angular momenta versus the rotational frequency. For an appropriate comparison with experiments, we plot the angular momentum over the whole SD yrast band (SD1 band). This coincides with the actual yrast band only for $\hbar\Omega > 0.67$ MeV.

V. COLLECTIVE EXCITATIONS AT NORMAL DEFORMATION AND SUPERDEFORMATION

We solved RPA Eqs. (6) under symmetry constraints (7) for each parity ($\pi = \pm$) and signature ($r = \pm 1$). These constraints ensure the separation of the redundant or spurious solutions from the physical ones on one hand, and, on the other hand, determine the strength constants of the multipole-multipole interactions. These constants came out to be close to the HO values [12]. We made a standard choice [12,36] for the remaining Hamiltonian parameters, the strengths of the spin-spin interaction. We completed the parameter set by using bare charges for the $E0$ and $E2$ transitions and a quenching factor $g_s = 0.7$ for the spin gyromagnetic ratios.

A. Low-lying octupole bands and the dynamical moment of inertia

Figure 4 shows how the lowest RPA energies, built on the SD yrast (SD1) band states as phonon vacua, evolve with the rotational frequency. In accordance with Ref. [4], the negative-parity RPA phonons are lowest in energy, because of the strong octupole correlations present in the SD states. One may note the crossing of the two lowest negative-parity bands with either positive or negative signature. These crossings have important effects on the dynamical moment of inertia. Since only the relative energies of the levels in the individual SD bands can be extracted from experiments [4,5,37], it is enough to compute the dynamical moments of inertia by use of the formula

$$\Im^{(2)}_\alpha(\Omega) = \Im^{(2)}_{\mathrm{yr}} - \frac{d^2E_\alpha}{d\Omega^2}, \tag{16}$$

where $\Im^{(2)}_{\mathrm{yr}}$ is the dynamical moment of inertia of the SD yrast band, which can be described approximately by the Harris formula

$$\Im^{(2)}_{\mathrm{yr}} = a + b\Omega^2. \tag{17}$$

The fit of the yrast band of ^{152}Dy yields for the above parameters $a = 88.5\hbar^2$ MeV^{-1} and $b = -11.9\hbar^4$ MeV^{-3}. The fluctuating part originates from the second derivative of the

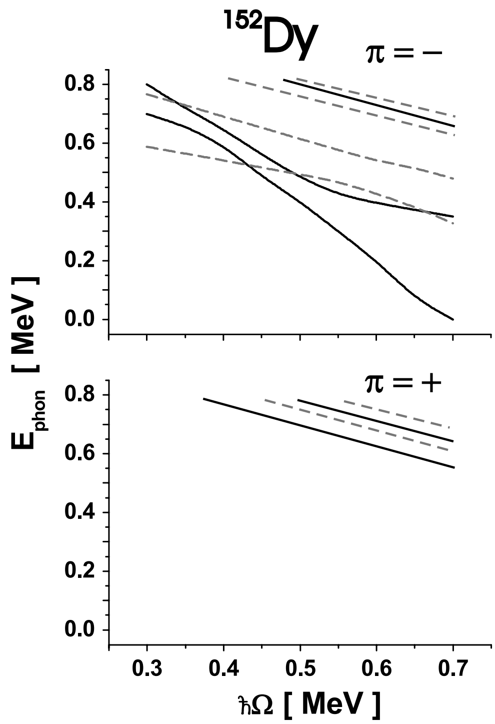

FIG. 4. Negative-parity (upper panel) and positive-parity (lower panel) lowest RPA intrinsic energies (routhians) versus rotational frequency. Solid and dashed lines correspond to positive and negative signatures, respectively.

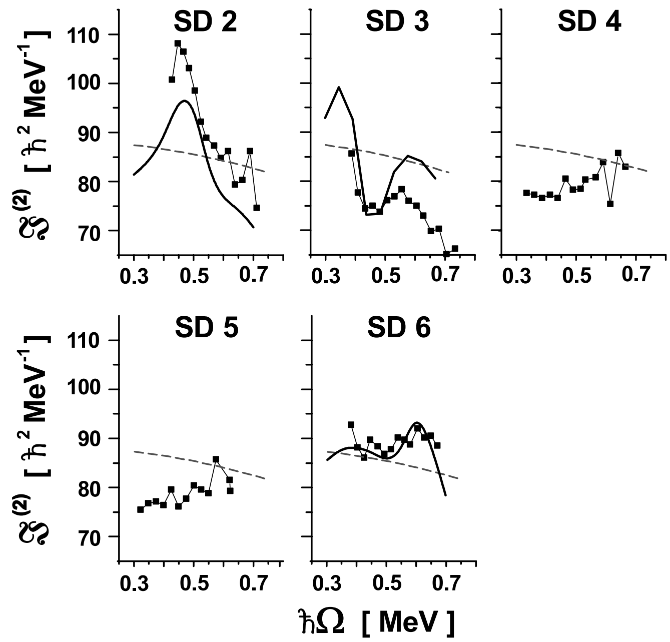

FIG. 5. The dynamical moments of inertia, determined by Eq. (16) (solid curves) are compared with the corresponding empirical values obtained from Eq. (18). The dashed curves correspond to the Harris fit [Eq. (17)].

phonon energy $E_{\text{phon}}(\Omega)$, which is a computed in RPA for a given band at different rotational frequencies.

The dynamical moment of inertia so defined is to be compared with the empirical one extracted from the energies $E_\alpha(I)$ of the SD bands α according to the formula

$$\Im_\alpha^{(2)}(\Omega) = \frac{4\hbar^2}{E_\alpha(I+4) - 2E_\alpha(I+2) - E_\alpha(I)}. \qquad (18)$$

The experimental energies are taken from [37] for all observed excited SD bands ($\alpha = \text{SD2, SD3, SD4, SD5, SD6}$). According to Eq. (16), only the moments of inertia of the negative-parity crossing bands, which yield nonzero second derivatives for the energy, should be appreciably affected by the rotation. This is confirmed empirically. As shown in Fig. 5, the dynamical moment of inertia, $\Im^{(2)}$, undergoes strong variations with Ω only for the negative parity and positive signature bands SD2,SD3 as well as for the negative parity and negative signature band SD6. The computed quantities are in fair agreement with the empirical moments of inertia of these three SD bands.

The fluctuations induced by the RPA phonons on the moments of inertia $\Im^{(2)}(\Omega)$ of the SD4 and SD5 bands are negligible, in qualitative agreement with experiments. The empirical quantities, in fact, undergo small oscillations and do not get far from the SD yrast values determined by the Harris formula (dashed curves). The RPA, however, is unable to reproduce the observed modest fluctuations, suggesting that they may be related to anharmonic effects.

It is important to point out that our results are fully consistent with the calculation and conclusions drawn in Ref. [4], where it was first pointed out the importance of the octupole correlations in shaping the dependence of the dynamical moment of inertia with rotational frequency in SD nuclei.

B. Electric and magnetic responses and the scissors mode

Fast rotation together with shape transition have a deep impact on the other electric and magnetic responses. Of considerable importance for our purposes are the changes induced by rotation plus deformation on the $E1$ giant resonance. As shown in Fig. 6, the broad $E1$ peak around ∼15 MeV, at low energy and small deformation, gets broader with increasing β and Ω. As superdeformation sets in, the resonance gets damped and splits into two broad branches, the more prominent $K^\pi = 0^-$ hump around 10–11 MeV and the $K^\pi = 1^-$ peak around 22–23 MeV.

As shown in Fig. 7, the $E0$ spectrum exhibits a well-pronounced peak, which remains around 18 MeV for all values of β and Ω until the point of transition to superdeformation is reached. With the onset of superdeformation, the $E0$ strength gets damped and fragmented while the (quenched) peak moves upward by a few mega-electron-volts.

The $E2$ spectrum (Fig. 8) shows some sensitivity also at small deformations and low rotational frequencies. Its main peak becomes more spread as the nucleus undergoes the first shape transition and the rotational frequency increases. It is dramatically damped and shifted upward by several mega-electron-volts as soon as the nucleus reaches the point of transition to superdeformation. In this new regime,

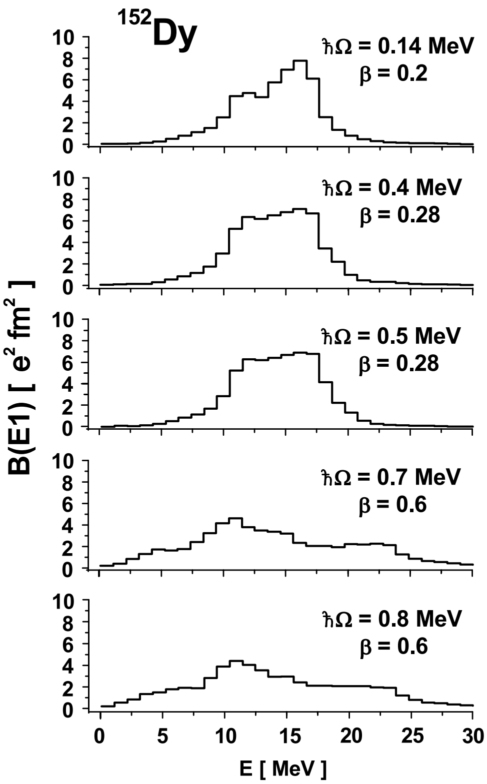

FIG. 6. $E1$ strength distribution for different angular frequencies and deformations. The reduced strengths are summed in bins of 1 MeV around the energy E of the final state excited from the yrast band.

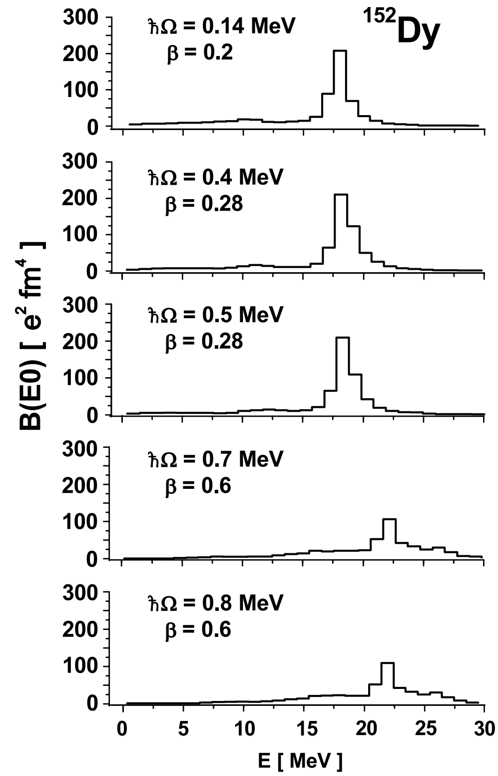

FIG. 7. $E0$ spectra for different angular frequencies and deformations. The reduced strengths are summed in bins as in Fig. 6.

the spectrum shows little sensitivity to rotation. It might be worth noting that the much smaller, high-energy isovector peak, clearly noticeable at normal deformation, is quickly swept away as rotation and deformation increase.

The behavior of the $M1$ response appears to be quite intriguing. Most of the $M1$ strength remains concentrated in the energy range 2–10 MeV at all frequencies and deformations (Fig. 9). At low rotational frequency and normal deformation ($\beta = 0.2$), most of the strength is due to spin excitations. It is only in the low-energy tail (2–4) MeV that the orbital contribution is comparable with the one that is due to spin.

The first shape transition ($\beta = 0.2 \rightarrow \beta = 0.28$) induces an overall enhancement of the orbital transition, especially at low energy, with a consequent downward shift of the total $M1$ strength. For fixed deformation, rotation has a damping effect on spin and affects marginally the orbital strength.

The onset of superdeformation induces more dramatic changes. It enhances strongly the orbital strength, which becomes strongly peaked around 6 MeV and has a damping and spreading effect on spin transitions, which get scattered all along the 2–10 MeV interval. The shape and peak of the total $M1$ strength distribution are determined almost solely by the orbital response. Rotation no longer affects appreciably either the orbital or the spin motion once the nucleus is settled down in the SD phase. The low-lying orbital strength amounts to $\sim 20\mu_N^2$ (Fig. 10). Although scattered, the low-lying spin transitions carry an appreciable strength, amounting to $\sim 10\mu_N^2$. Orbital and spin amplitudes interfere constructively, yielding a total $M1$ strength of $\sim 30\mu_N^2$.

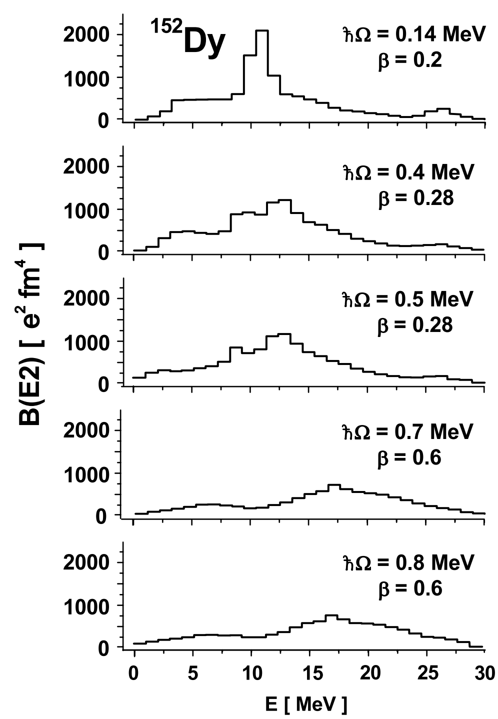

FIG. 8. $E2$ spectra for different angular frequencies and deformations. The reduced strengths are summed in bins as in Fig. 6.

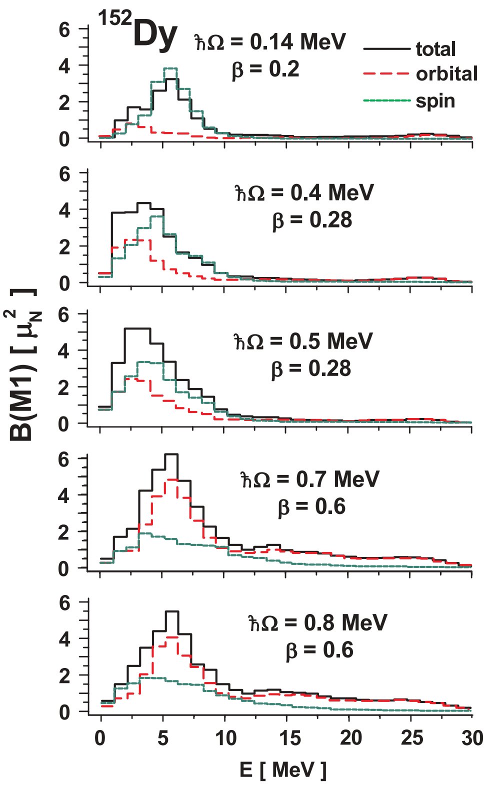

FIG. 9. (Color online) $M1$ spectra for different angular frequencies and deformations. The reduced strengths are summed in bins as in Fig. 6.

A high-energy peak, which can hardly be noticed at normal deformation, is well noticeable in the SD phase. It is rather broad and carries a $M1$ strength of only $\sim 5\mu_N^2$, much smaller than the the one collected by the low-energy excitations.

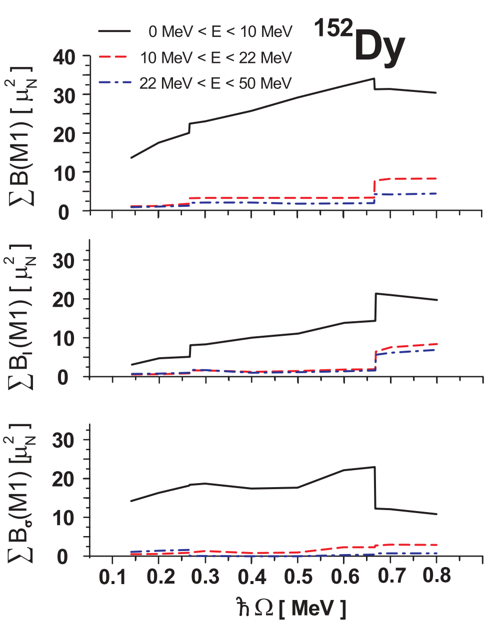

FIG. 10. (Color online) $M1$ strengths partially summed over three distinct energy ranges. The corresponding orbital and spin contributions are plotted in the middle and lower panels, respectively.

The present calculation converges with the one performed in Ref. [7] at some points, but diverges strongly at others. Consistent with Ref. [7], we find a spin dominance at normal deformation as well as an enhancement of the orbital over the spin strength as we move from normal deformation to superdeformation. More quantitatively, the low-lying orbital strength ($\sim 20\mu_N^2$) approaches from below the value $23\mu_N^2$ obtained in Ref. [7]. The spin strength computed in Ref. [7], instead, though comparable in magnitude with the one obtained here, is much more strongly peaked.

Our high-energy $M1$ strength ($\sim 5\mu_N^2$) is far smaller than the huge value, $37\mu_N^2$, obtained in Ref. [7]. Moreover, it is considerably spread over a range of several mega-electron-volts, contrary to the findings of Ref. [7], in which the whole strength is concentrated into a single narrow peak. The latter feature, however, was admittedly ascribed to the restricted single-particle space adopted, which allowed for only two quasiparticle energies up to 20 MeV.

The large discrepancy between the two calculations concerning the high-nergy $M1$ response is rather puzzling. It may be partly related to the much larger single-particle space we use to reach the equilibrium deformation and to the combined action of deformation and rotation, neglected in Ref. [7]. It is unlikely, however, that these two factors can determine such different responses. The difference cannot be ascribed to our Nilsson parametrization. We have checked that the distribution and magnitude of the $M1$ and the other strengths change little if we use standard Nilsson parameters [32].

We conclude that, according to our calculation, rotation plus superdeformation have the main effect of enhancing strongly the low-lying orbital $M1$ transitions over the spin. The orbital response determines the shape and peak of the strength distribution and therefore qualifies the low-lying $M1$ excitations as scissors mode.

To further test this assertion, we put the $m_1(M1)$ moment, yielding the energy-weighted sum of the $M1$ strengths, in relation to the kinematical moment of inertia $\Im^{(1)}$. These two quantities should be intimately correlated if the $M1$ excitations have a scissors nature. For these kinds of transitions, in fact, the following energy-weighted sum rule holds [38,39]:

$$m_1(M1)^{(\mathrm{sc})} = \sum_n (E_n - E_0) B_n^{(\mathrm{sc})}(M1) = \frac{3}{16\pi}\Im^{(1)}\omega^2, \quad (19)$$

where ω is the centroid of the scissorslike excitations.

As shown in Fig. 11, not only the orbital but also the total $M1$ moments follow closely the moment of inertia in its evolution with β and Ω. Like $\Im^{(1)}$, they jump at the phase transition points and remain practically constant in between. Because of such a close link with $\Im^{(1)}$, the low-lying $M1$ excitations in SD nuclei are to be associated with the scissors mode. The high-lying $M1$ peak corresponds to the high-energy scissors mode. This, however, being rather weakly excited, is of little relevance for experimental purposes.

It is, instead, of considerable interest to explore the possibility of detecting the low-energy scissors mode in decay processes. This is actually the collective mode that is lowest in

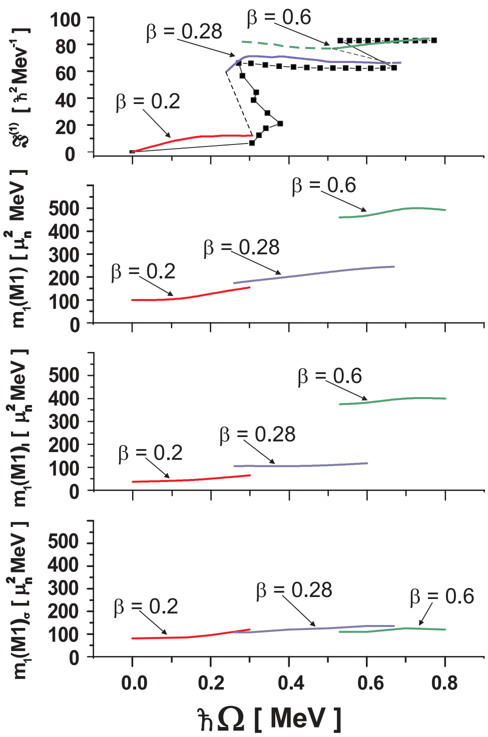

FIG. 11. (Color online) The yrast line kinematical moment of inertia (upper panel) versus the total (second panel), orbital (third panel), and spin (bottom panel) $m_1(M1)$ moments.

energy, apart from the octupole states. Indeed, the $M1$ peak is well below the humps of the $E0$ and $E2$ resonances and also below the $K^\pi = 0^-$ $E1$ giant resonance peak at ~10 MeV. It overlaps only with the low-lying queues of the $E2$ and the $K^\pi = 0^-$ $E1$ resonances. On the other hand, the methods of analysis of γ-cascade spectra have improved considerably in recent years. Indeed, these methods have proved to be quite successful in disentangling the $M1$ from the $E\lambda$ excitations, thereby, detecting for the first time the scissors mode built on excited states in slowly rotating nuclei [40].

VI. CONCLUSIVE REMARKS

We have shown that, through adopting a cranked Nilsson mean field, our QRPA approach ensures the separation of the spurious or redundant solutions from the physical ones. The evolution of the dynamical moment of inertia with increasing deformations and rotational frequencies confirms the conclusion drawn in Refs. [4,5] about the octupole character of the negative-parity excited SD bands near the yrast line. Our analysis shows that the onset of superdeformation has a strong impact on the other electric collective modes and, to a much higher degree, on the orbital $M1$ response. This is dramatically enhanced over the spin around 6 MeV above the yrast line and confers to these low-lying $M1$ transitions the typical features of the scissors mode. Being the lowest in energy, apart from the octupole excitations, such a mode should have a good chance of being detected in γ-cascade processes, thanks to the very effective modern methods of analysis of the decay spectra. We are confident that the present results remain valid even in a more realistic Nilsson-Strutinsky approach. We found, indeed, that our collective responses are rather insensitive to changes in the Nilsson parameters.

ACKNOWLEDGMENTS

This work was partly supported by the Italian Ministero dell'Istruzione, Universitá and Ricerca and is part of the research plan MSM 0021620834 supplied by the Ministry of Education of the Czech Republic.

[1] P. J. Twin, B. M. Nyakó, A. H. Nelson, J. Simpson, M. A. Bentley, H. W. Cranmer-Gordon, P. D. Forsyth, D. Howe, A. R. Mokhtar, J. D. Morrison, J. F. Sharpey-Schafer, and G. Sletten, Phys. Rev. Lett. **57**, 811 (1986).
[2] W. Nazarewicz, R. Wyss, and A. Johnson, Nucl. Phys. **A503**, 285 (1989).
[3] Y. R. Shimizu, E. Viggezi, and R. A. Broglia, Nucl. Phys. **A509**, 80 (1990).
[4] T. Nakatsukasa, K. Matsuyanagi, S. Mizutori, and W. Nazarewicz, Phys. Lett. **B343**, 19 (1995).
[5] T. Nakatsukasa, K. Matsuyanagi, S. Mizutori, and Y. R. Shimizu, Phys. Rev. C **53**, 2213 (1996).
[6] S. Mizutori, Y. R. Shimizu, and K. Matsuyanagi, Prog. Theor. Phys. **83**, 666 (1990); **85**, 559 (1991); **86**, 131 (1991).
[7] I. Hamamoto and W. Nazarewicz, Phys. Lett. **B297**, 25 (1992).
[8] N. Lo Iudice and F. Palumbo, Phys. Rev. Lett. **41**, 1532 (1978).
[9] D. Bohle, A. Richter, W. Steffen, A. E. L. Dieperink, N. Lo Iudice, F. Palumbo, and O. Scholten, Phys. Lett. **B137**, 27 (1984).
[10] For an exhaustive list of references, see N. Lo Iudice, Riv. Nuovo Cimento **23**, 1 (2000).
[11] N. Lo Iudice and A. Richter, Phys. Lett. **B228**, 291 (1989).
[12] J. Kvasil, N. Lo Iudice, R. G. Nazmitdinov, A. Porrino, and F. Knapp, Phys. Rev. C **69**, 064308 (2004).
[13] S. Aberg, Nucl. Phys. **A473**, 1 (1987).
[14] E. R. Marshalek, Phys. Rev. C **11**, 1426 (1975); Nucl. Phys. **A266**, 317 (1976).
[15] J. L. Egido, H. J. Mang, and P. Ring, Nucl. Phys. **A339**, 390 (1980).
[16] Y. R. Shimizu and K. Matsuyanagi, Prog. Theor. Phys. **70**, 144 (1983); **72**, 799 (1984).
[17] P. Ring, L. M. Robledo, J. L. Egido, and M. Faber, Nucl. Phys. **A419**, 261 (1984).
[18] Y. R. Shimizu and K. Matsuyanagi, Prog. Theor. Phys. **75**, 1161 (1986).
[19] L. M. Robledo, J. L. Egido, and P. Ring, Nucl. Phys. **A449**, 201 (1986).
[20] S. Mizutori, Y. R. Shimizu, and K. Matsuyanagi, Prog. Theor. Phys. **83**, 666 (1990); **85**, 559 (1991); **86**, 131 (1991).
[21] T. Nakatsukasa, S. Mizutori, and K. Matsuyanagi, Prog. Theor. Phys. **87**, 607 (1992); **89**, 847 (1993).
[22] S. Mizutori, T. Nakatsukasa, K. Arita, Y. R. Shimizu, and K. Matsuyanagi, Nucl. Phys. **A557**, 125c (1993).

[23] T. Nakatsukasa, K. Matsuyanagi, S. Mizutori, and W. Nazarewicz, Phys. Lett. **B343**, 19 (1995).
[24] Y. R. Shimizu and K. Matsuyanagi, Nucl. Phys. **A588**, 559 (1995).
[25] J. Kvasil, and R. G. Nazmitdinov, Phys. Rev. C **69**, 031304(R) (2004).
[26] E. R. Marshalek, Phys. Rev. Lett. **51**, 1534 (1983).
[27] E. R. Marshalek, Phys. Rev. C **29**, 640 (1984).
[28] J. Kvasil, N. Lo Iudice, V. O. Nesterenko, and M. Kopal, Phys. Rev. C **58**, 209 (1998).
[29] T. Kishimoto, J. M. Moss, D. H. Youngblood, J. D. Bronson, C. M. Rozsa, D. R. Brown, and A. D. Bacher, Phys. Rev. Lett. **35**, 552 (1975).
[30] H. Sakamoto and T. Kishimoto, Nucl. Phys. **A501**, 205 (1989).
[31] A. K. Jain, R. K. Sheline, P. C. Sood, and K. Jain, Rev. Mod. Phys. **62**, 393 (1990).
[32] T. Bengtsson and I. Ragnarsson, Nucl. Phys. **A436**, 14 (1985).
[33] R. Wyss, W. Satula, and W. Nazarewicz, Nucl. Phys. **A511**, 324 (1990).
[34] Y. R. Shimizu and K. Matsuyanagi, Prog. Theor. Phys. **71**, 960 (1984).
[35] B. Singh, Nucl. Data Sheets **95**, 995 (2002); http://www.nndc.bnl.gov/nudat2/
[36] B. Castel and I. Hamamoto, Phys. Lett. **65B**, 27 (1976).
[37] P. J. Dagnall, C. W. Beausang, P. J. Twin, M. A. Bentley, F. A. Beck, Th. Byrski, S. Clarke, D. Curien, G. Duchene, G. de France, P. D. Forsyth, B. Haas, J. C. Lisle, E. S. Paul, J. Simpson, J. Styczen, J. P. Vivien, J. N. Wilson, and K. Zuber, Phys. Lett. **B335**, 313 (1994).
[38] E. Lipparini and S. Stringari, Phys. Lett. **B130**, 139 (1984)
[39] N. Lo Iudice, Phys. Rev. C **57**, 1246 (1998).
[40] M. Krticka, F. Becvar, J. Honzatko, I. Tomandl, M. Heil, F. Kappeler, R. Reifarth, F. Voss, and K. Wisshak, Phys. Rev. Lett. **92**, 172501 (2004).